



Title	All-Optical Diode Suppressing Broadband Backward Transmission Using Single- and Four-Port Photonic Crystal Cavities
Author(s)	Sato, Takanori; Fujisawa, Takeshi; Saitoh, Kunimasa
Citation	IEEE photonics journal, 11(1), 4900214 https://doi.org/10.1109/JPHOT.2018.2888632
Issue Date	2019-02
Doc URL	http://hdl.handle.net/2115/72995
Rights	© 2018 IEEE. Personal use of this material is permitted. Permission from IEEE must be obtained for all other uses, in any current or future media, including reprinting/republishing this material for advertising or promotional purposes, creating new collective works, for resale or redistribution to servers or lists, or reuse of any copyrighted component of this work in other works.
Type	article
File Information	08581445.pdf

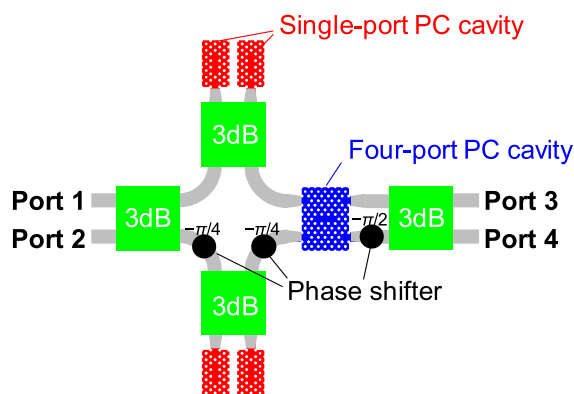


[Instructions for use](#)

All-Optical Diode Suppressing Broadband Backward Transmission Using Single- and Four-Port Photonic Crystal Cavities

Volume 11, Number 1, February 2019

Takanori Sato, *Member, IEEE*
Takeshi Fujisawa, *Member, IEEE*
Kunimasa Saitoh, *Member, IEEE*



DOI: 10.1109/JPHOT.2018.2888632
1943-0655 © 2018 IEEE

All-Optical Diode Suppressing Broadband Backward Transmission Using Single- and Four-Port Photonic Crystal Cavities

Takanori Sato , Member, IEEE, Takeshi Fujisawa , Member, IEEE, and Kunimasa Saitoh , Member, IEEE

Graduate School of Information Science and Technology, Hokkaido University, Sapporo
060-0814, Japan

DOI:10.1109/JPHOT.2018.2888632

1943-0655 © 2018 IEEE. Translations and content mining are permitted for academic research only.
Personal use is also permitted, but republication/redistribution requires IEEE permission.
See http://www.ieee.org/publications_standards/publications/rights/index.html for more information.

Manuscript received November 6, 2018; accepted December 14, 2018. Date of publication December 19, 2018; date of current version January 9, 2019. This work was supported by JSPS KAKENHI under Grant JP17J00378. Corresponding author: Takanori Sato (e-mail: tsato@icp.ist.hokudai.ac.jp).

Abstract: We present an all-optical diode suppressing broadband backward transmission using single-port and four-port photonic crystal (PC) cavities and its operation principle. We find that, by combining a four-port PC cavity and two power-dependent phase shifters that are composed by a 3-dB power divider and two single-port PC cavities, the backward transmission in the nonlinear-resonator-based all-optical diode becomes theoretically 0% for any input power and any input wavelength. To confirm the validity of our approach, the numerical analysis based on the nonlinear beam propagation method as well as the coupled mode theory is performed. The results prove that the forward transmission of -4 dB and large nonreciprocal transmission ratio of 35 dB are achievable.

Index Terms: Photonic crystal cavity, resonator, all-optical device, and nonlinear optics.

1. Introduction

All-optical signal processing that is controlling the optical signals by their nonlinear effects could be a key technology for the ultrafast and high-capacity data communication. So far, many types of the all-optical devices including the switches [1], [2], memories [3], [4], logic gates [5], [6], and diodes [7]–[10], have been experimentally demonstrated by the micro-ring resonators and photonic crystal (PC) cavities. In particular, the nonlinear-resonator-based all-optical diodes can exhibit the one-way transmission characteristics on silicon-on-insulator platform (SOI) without magneto-optical materials, which is an advantage in terms of CMOS compatibility. Although the all-optical diodes have a dynamic reciprocity [11], it is useful as a simple pulse isolator [9] and contributes to the diversity of functionalities for the electronic-photonic chip. In the conventional nonlinear-resonator-based all-optical devices, the operation principle is based on the nonlinear shift of the resonant transmission peak, which is occurred by the third-order nonlinear effects including the optical Kerr-effect, the carrier plasma effect, and the thermo-optical effect. For example, by cascading the different nonlinear resonators, the nonlinear resonant shift in each resonator vary for the propagation direction, which leads the nonreciprocal characteristics [12]. L. Fan *et al.* reported the large nonreciprocal transmission ratio (NTR) of 40 dB by the cascaded Si ring resonators [8], which is the largest experimentally obtained NTR to our knowledge. However, if the wavelength or power of input lightwave is slightly detuned from designed value, the backward transmission is easily emerged. Recently, C.

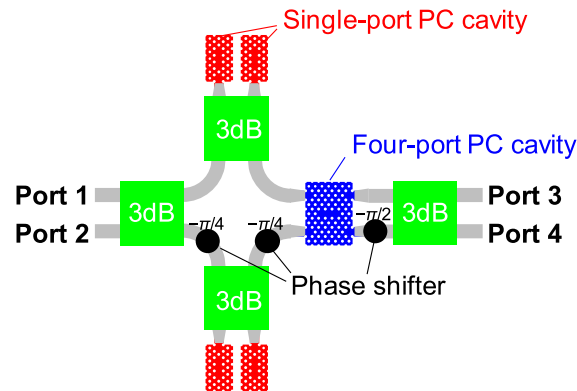


Fig. 1. Schematic of a newly proposed all-optical diode. The green, red, blue, and black illustrations denote 3-dB power divider, single-port PC cavity, four-port PC cavity, and static PS, respectively.

Li *et al.* numerically demonstrated the broadband all-optical diode [13], which is composed by two PC cavities that have the Q -factor of about 1000, and reported the NTR of 25 dB and bandwidth of 2 nm. Nevertheless, the backward transmission is emerged out of the bandwidth. As long as we rely on the conventional nonlinear-resonator-based operation principle, it seems to be difficult to completely block the backward transmission. For that reason, we try to exploit the nonreciprocal characteristics from the nonlinear modulation of the phase of the reflection coefficient instead of the nonlinear modulation of the transmission spectrum peak. More recently, we find the design of the all-optical diode that can completely suppress the backward input lightwave for any input power and for any input wavelength although it has also the dynamic reciprocity [14]. However the proposed device is very complicated as shown in Fig. 1. It is composed by four 3-dB power divider, four single-port PC cavities, one four-port PC cavity, and three static phase shifters (PSs), which correspond to the green, red, blue, and black illustrations in the figure, respectively. The single-port PC cavity and four-port cavity, which are uncommon and unique components, play important role in the operation principle. This time, we presents the detailed operation principle and the numerical results calculated by coupled mode theory (CMT) and finite-element time-domain beam propagation method (FETD-BPM).

In this paper, to explain the principle of our proposed device, the basic characteristic of each component in the device is first explained in Section 2. Here, we also explain the modulation of the phase of the reflection coefficient in the power-dependent PS (PDPS) that is composed by two single-port PC cavities and a 3-dB power divider. In Section 3, the operation principle of the proposed all-optical diode is shown. Furthermore, the numerical results by CMT and FETD-BPM are shown. It proves that the all-optical diode can achieve the broadband suppression of the backward transmission and extremely large NTR since the backward transmission should be theoretically 0%.

2. Basic Characteristics of Components

2.1 3-dB Power Divider

The 3-dB power divider equally divides the one guided mode into two guided modes. It can be easily realized by a multimode interferometer (MMI) coupler [15]–[18] or a directional coupler [19]–[21]. The MMI coupler is robust to an fabrication error and has broadband characteristics [15]. Whereas, the directional coupler has extremely low-loss insertion loss and its bandwidth can be easily improved [20], [21]. In addition, we can directly express the detailed transmission characteristics of the 3-dB power divider by using the CMT analysis. For that reason, here we choose the directional coupler as a 3-dB power divider.

Fig. 2(a) shows the schematic of the single-mode and symmetric directional coupler, where β is a propagation constant, κ is a coupling coefficient, L is a propagation length, and a_i and b_i are

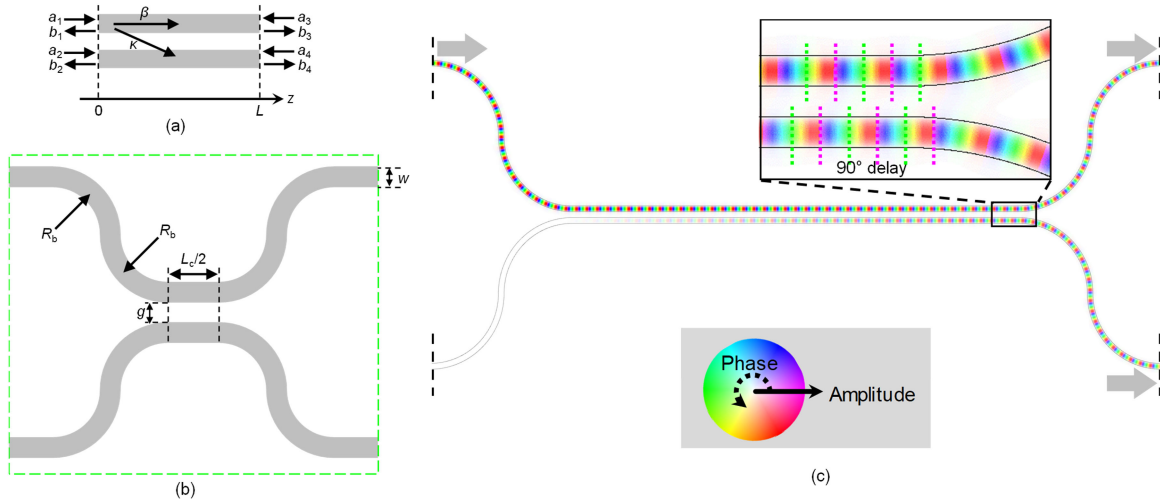


Fig. 2. Schematic of (a) the single-mode and symmetric directional coupler and (b) it connected to the routing 90-degree bent waveguide for the separation. (c) Numerical example of the magnetic field according to (b), where $w = 400$ nm, $g = 400$ nm, $L_c = 63 \mu\text{m}$, $R_b = 5 \mu\text{m}$, and the refractive index of the core and cladding materials are 2.76 (effective index of Si) and 1 (air), respectively.

incoming and outgoing amplitudes on i th port, respectively. According to CMT equation for the directional coupler [19], the evolution of the amplitudes can be expressed as

$$\frac{d}{dz} \begin{bmatrix} a_1 \\ a_2 \end{bmatrix} = -j \begin{bmatrix} \beta & \kappa \\ \kappa & \beta \end{bmatrix} \begin{bmatrix} a_1 \\ a_2 \end{bmatrix} = -\frac{j}{2} \begin{bmatrix} 1 & 1 \\ 1 & -1 \end{bmatrix} \begin{bmatrix} \beta + \kappa & 0 \\ 0 & \beta - \kappa \end{bmatrix} \begin{bmatrix} 1 & 1 \\ 1 & -1 \end{bmatrix} \begin{bmatrix} a_1 \\ a_2 \end{bmatrix} \quad (1)$$

and the transfer matrix is derived as

$$\begin{aligned} \begin{bmatrix} b_3 & b_4 \end{bmatrix}^T &= \mathbf{T}_{\text{DC}}(L) \begin{bmatrix} a_1 & a_2 \end{bmatrix}^T, \\ \mathbf{T}_{\text{DC}}(L) &= \frac{1}{2} \begin{bmatrix} 1 & 1 \\ 1 & -1 \end{bmatrix} \begin{bmatrix} \exp[-j(\beta + \kappa)L] & 0 \\ 0 & \exp[-j(\beta - \kappa)L] \end{bmatrix} \begin{bmatrix} 1 & 1 \\ 1 & -1 \end{bmatrix} \\ &= \exp(-j\beta L) \begin{bmatrix} \cos(\kappa L) & -j\sin(\kappa L) \\ -j\sin(\kappa L) & \cos(\kappa L) \end{bmatrix}. \end{aligned} \quad (2) \quad (3)$$

Clearly seen from Eqs. (2) and (3), the coupling length is given by $L_c = \pi/(2\kappa)$ and the length for 3-dB power divider is given by $L_{3\text{dB}} = L_c/2$. Substituting $L = L_{3\text{dB}}$ into Eq. (3), we can obtain the transfer matrix for the 3-dB power divider as

$$\mathbf{T}_{3\text{dB}} = \mathbf{T}_{\text{DC}}(L_{3\text{dB}}) = \frac{\exp(-j\beta L_{3\text{dB}})}{\sqrt{2}} \begin{bmatrix} 1 & \exp(-j\pi/2) \\ \exp(-j\pi/2) & 1 \end{bmatrix}, \quad (4)$$

where we can find the 90-degree difference between the divided modes. The other complex amplitudes can be also expressed in the same way, and hence the scattering matrix is derived as

$$\begin{bmatrix} b_1 & b_2 & b_3 & b_4 \end{bmatrix}^T = \mathbf{S}_{3\text{dB}} \begin{bmatrix} a_1 & a_2 & a_3 & a_4 \end{bmatrix}^T, \quad (5)$$

$$\mathbf{S}_{3\text{dB}} = \frac{\exp(-j\beta L_{3\text{dB}})}{\sqrt{2}} \begin{bmatrix} 0 & 0 & 1 & -j \\ 0 & 0 & -j & 1 \\ 1 & -j & 0 & 0 \\ -j & 1 & 0 & 0 \end{bmatrix}. \quad (6)$$

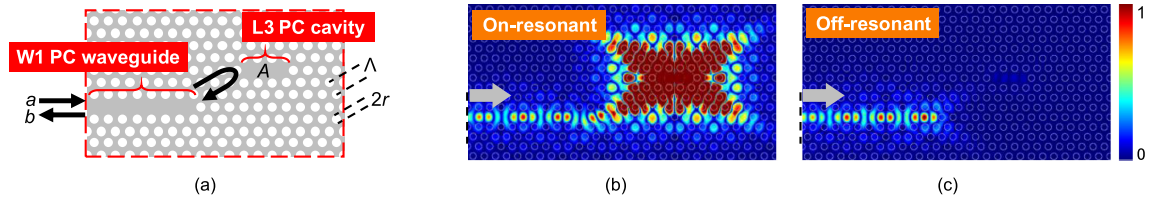


Fig. 3. (a) Schematic of the single-port cavity and its (b) on-resonant and (c) off-resonant field distributions, where $\Lambda = 420$ nm, $r = 0.29\Lambda$, and the refractive index of the slab and hole materials are 2.76 and 1, respectively. (Colormap is normalized as the maximum amplitude in the waveguide and larger amplitude is rounded to 1.)

To separate two waveguides, the directional coupler is symmetrically connected to the routing 90-degree bent waveguides as shown in Fig. 2(b), where w is a waveguide width, g is a gap between two waveguides, and R_b^{-1} is a curvature of bent waveguide. Fig. 2(c) shows the numerical example of the magnetic field according to Fig. 2(b), where $w = 400$ nm, $g = 400$ nm, $L_c = 63$ μ m, $R_b = 5$ μ m, and the refractive index of the core and cladding materials are 2.76 (effective index of Si [22]) and 1 (air), respectively. To focus on the phase distribution, we show the field distribution using HSV (Hue-Saturation-Value) colormap that can express amplitude (saturation) and phase (hue) simultaneously. We can confirm the 90-degree phase delay for the cross port transmission from Fig. 2(c) as well as Eq. (4).

2.2 Single-Port PC Cavity

Figs. 3(a)–(c) show the schematics of the single-port PC cavity and its on-resonant and off-resonant magnetic field distributions. It is composed by the single-line-defect (W1) waveguide and the three-hole-defect (L3) cavity, where Λ is a lattice constant, r is a hole radius, and a and b are incoming and outgoing amplitudes, respectively. For simplicity, we neglect the intrinsic loss of the cavity mode, and hence the reflection becomes always 100% for any input wavelength. However, the phase of the reflection coefficient strongly depends on the difference between input and resonant wavelength. To investigate the nonlinear characteristics of a single-port PC cavity as shown in Fig. 3, we directly solve the following ordinary differential coupled mode equations according to the resonant amplitude A [12], [19]:

$$\frac{d}{dt}A(t) = \left(j\omega_{\text{NL}} - \frac{1}{\tau}\right)A(t) + \sqrt{\frac{2}{\tau}}a, \quad (7)$$

$$\omega_{\text{NL}} = \omega_0 \frac{n_0}{n_0 + \gamma|A(t)|^2} \quad (8)$$

$$b = -a + \sqrt{\frac{2}{\tau}}A(t), \quad (9)$$

where τ^{-1} is a decay rate, ω_0 is a linear resonant frequency, ω_{NL} is a nonlinear resonant frequency, n_0 is a linear refractive index of core, and γ is a nonlinear parameter. The decay rate is related to the quality factor as $Q = \omega_0\tau$. We assume the optical Kerr effect as the main factor for the resonant peak shift and it is taken into account by γ . The reflection coefficient is given by $R = b/a$, where we omit the roundtrip phase shift in the W1 PC waveguide. If the resonator is linear ($\gamma = 0$), the stationary solution of A and the reflection coefficient R are derived as

$$A|_{\gamma=0} = \left[j(\omega_{\text{in}} - \omega_0) + \frac{1}{\tau}\right]^{-1} \sqrt{\frac{2}{\tau}}a \quad (10)$$

$$R|_{\gamma=0} = \frac{1 - j(\omega_{\text{in}} - \omega_0)\tau}{1 + j(\omega_{\text{in}} - \omega_0)\tau} \quad (11)$$

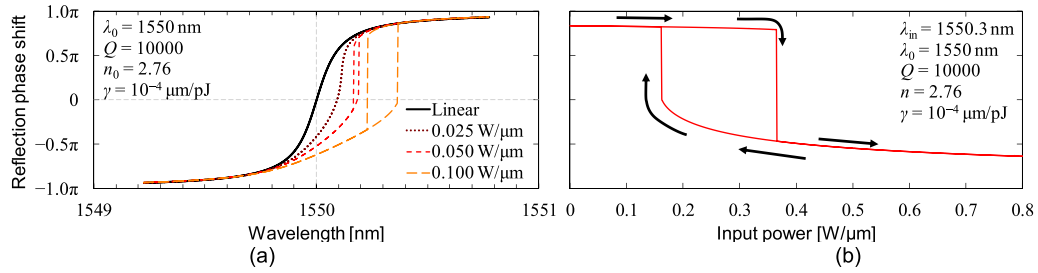


Fig. 4. Reflection characteristics of the single-port PC cavity calculated from Eqs. (7)–(9). (a) The phase of reflection coefficient R as a function of input wavelength for various input powers. (b) The phase of reflection coefficient R as a function of input power.

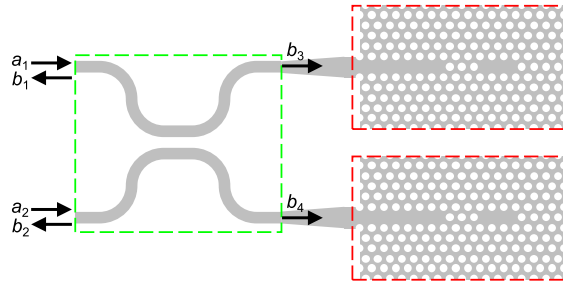


Fig. 5. Schematic of the two-port PDPS using one 3-dB power divider and two single-port PC cavities.

where ω_{in} is a frequency of the input source. As seen from Eq. (11), in the linear regime, the phase of reflection coefficient is determined by the detuning level. In the nonlinear regime, the detuning level depends on the input power, which means that the reflection coefficient R can be controlled by the input power. Fig. 4(a) shows the phase of reflection coefficient R , calculated from Eqs. (7)–(9), as a function of input wavelength for various input powers, where λ_0 ($= 2\pi c/\omega_0$) = 1550 nm, $Q = 10000$, $n_0 = 2.76$, and $\gamma = 10^{-4}$ $\mu\text{m}/\text{pJ}$. The parameters are similar to the previous work [12] and we assume the 2D structure. The unit of power ($|a|^2$, $|b|^2$) and energy ($|A|^2$) is divided by thickness, of which the direction is orthogonal to the 2D plane, and becomes W/m and J/m . The value of $\gamma = 10^{-4}$ $\mu\text{m}/\text{pJ}$ corresponds to the silicon L3 PC cavity that has the nonlinear refractive index of $n_2 = 6.0 \times 10^{-6}$ $\mu\text{m}^2/\text{W}$ and it is experimentally achievable value ($\gamma \approx 5 \times 10^{-4}$ $\mu\text{m}/\text{pJ}$ [23]). In Fig. 4(a), we can see the 360-degree phase difference between the on-resonant condition ($\omega_{\text{in}} = \omega_0$) and off-resonant condition ($\omega_{\text{in}} \ll \omega_0$ or $\omega_{\text{in}} \gg \omega_0$). If the resonant wavelength is red-shifted by the nonlinear effect, the phase of reflection coefficient R is also red-shifted, maintaining 100% reflection. Similar to the well-known bistable transmission characteristics [19], the phase of the reflection coefficient also has bistable state when the input power is sufficient large. Fig. 4(b) shows the phase of reflection coefficient R , calculated from Eqs. (7)–(9), as a function of input power, where input wavelength λ_{in} ($= 2\pi c/\omega_{\text{in}}$) is 1550.3 nm. An obvious hysteresis loop of the reflection phase shift appears for the input power of 0.16~0.37 $\text{W}/\mu\text{m}$. In such a single-port PC cavity, we can exploit the nonlinear bistable state without changing the reflection power and it is difficult to realize such operation by using ring resonators instead of PC cavities.

2.3 Two-Port PDPS

By combining two single-port PC cavities with a 3-dB power divider, we can construct a two-port PDPS as shown in Fig. 5, where we deploying the tapered wire waveguide to match the waveguide

TABLE 1
Relationship between a_i and b_i in the PDPS

	Input amplitude		Power flowing into cavity		Output amplitude	
	a_1	a_2	$P_3 (= b_3 ^2)$	$P_4 (= b_4 ^2)$	b_1	b_2
(i)	1	0	1/2	1/2	0	$\exp(-j\pi/2)$
(ii)	0	1	1/2	1/2	$\exp(-j\pi/2)$	0
(iii)	1	1	1	1	$\exp(-j\pi/2)$	$\exp(-j\pi/2)$
(iv)	1	-1	1	1	$-\exp(-j\pi/2)$	$\exp(-j\pi/2)$
(v)	1	$\exp(+j\pi/2)$	1	0	1	$\exp(-j\pi/2)$
(vi)	1	$\exp(-j\pi/2)$	0	1	-1	$\exp(-j\pi/2)$

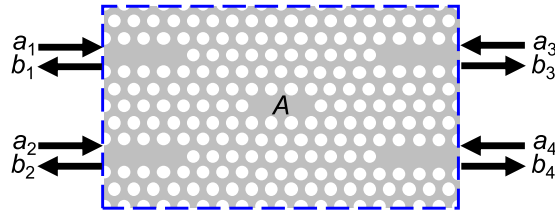


Fig. 6. Schematic of the four-port PC cavity.

widths. The scattering matrix of the two-port PDPS can be expressed as

$$[b_1 \ b_2]^T = \mathbf{S}_{\text{PDPS}} [a_1 \ a_2]^T, \quad (12)$$

$$\mathbf{S}_{\text{PDPS}} = \mathbf{T}_{3\text{dB}} \mathbf{T}_{1\text{PC}} \mathbf{T}_{3\text{dB}} = \frac{1}{2} \begin{bmatrix} R_1 - R_2 & -j(R_1 + R_2) \\ -j(R_1 + R_2) & -R_1 + R_2 \end{bmatrix} \quad (13)$$

$$\mathbf{T}_{1\text{PC}} = \begin{bmatrix} R_1 & 0 \\ 0 & R_2 \end{bmatrix} \quad (14)$$

where R_1 and R_2 are the reflection coefficient of the upper and lower single-port PC cavities, respectively. Table 1 summarizes the relationship between input amplitudes $a_{1,2}$ and other amplitude $b_{1,2,3,4}$. If the lightwave is input from one arm waveguide((i) and (ii) in Table 1), the half power flows equally into each cavities, and the whole power escapes to the other arm waveguide due to the interference in the 3-dB power divider. Here let us consider the power flowing when the lightwaves are simultaneously input from both the upper-left and lower-left ports. If the in-phase or out-phase amplitude is input ((iii) and (iv)), we can find that the same power ($|b_3|^2 = |b_4|^2 = 1$) flows into upper and lower cavities. Whereas, if the 90-degree different amplitude input ((v), (vi)), we can find that the power flows into one cavity and the other cavity completely do not receive any power. We should keep in mind that, in the nonlinear regime, the phase of the reflection coefficient $R_{1,2}$ in the cavity is considerably affected by the power flowing into cavity, namely, the phase difference between a_1 and a_2 .

2.4 Four-Port PC Cavity

Here we assume that the cavity is a four-port L3 cavity that is symmetrically connected to four W1 waveguides as shown in Fig. 6. Similar to Eq. (7), the coupled mode equation for resonant

TABLE 2
Relationship between a_i and b_i in the Four-Port PC Cavity

	Input amplitude				Output amplitude			
	a_1	a_2	a_3	a_4	b_1	b_2	b_3	b_4
(i)	+1	+1	0	0	0	0	-1	-1
(ii)	+1	-1	0	0	-1	+1	0	0
(iii)	0	0	+1	+1	-1	-1	0	0
(iv)	0	0	+1	-1	0	0	-1	+1

amplitude A is given by [12], [19]:

$$\frac{d}{dt}A(t) = \left[j\omega_{\text{NL}} - \sum_{i=1}^4 \left(\frac{1}{\tau} \right) \right] A(t) + \sum_{i=1}^4 \left(\sqrt{\frac{2}{\tau}} p_i a_i \right), \quad (15)$$

$$b_i = -a_i + p_i \sqrt{\frac{2}{\tau}} A(t), \quad (16)$$

where p_i denote a symmetry sign for the i th port. Especially for the fundamental resonant mode in the L3 cavity as shown in Fig. 6, the magnetic field is odd symmetry to the vertical axis and even symmetry to the horizontal axis, resulting $p_1 = p_2 = -p_3 = -p_4 = 1$. Therefore, the scattering matrix can be expressed as

$$[b_1 \ b_2 \ b_3 \ b_4]^T = \mathbf{S}_{4\text{PC}} [a_1 \ a_2 \ a_3 \ a_4]^T \quad (17)$$

$$\mathbf{S}_{4\text{PC}} = \frac{1}{1-\eta} \begin{bmatrix} \eta & 1 & -1 & -1 \\ 1 & \eta & -1 & -1 \\ -1 & -1 & \eta & 1 \\ -1 & -1 & 1 & \eta \end{bmatrix} \quad (18)$$

$$\eta = -1 + j \frac{(\omega_{\text{NL}} - \omega_{\text{in}}) \tau}{2} \quad (19)$$

In the proposed device, we design the low Q-factor four-port PC cavity compared with the Q-factor of the single-port PC cavities in PDPSS and the resonance wavelength is almost the same as input wavelength, which leads $\eta \approx -1$ from Eq. (19). In such condition, we can find that the four-port PC cavity is available as a linear logic gate that gives the response as shown in Table 2. For example, if an in-phase lightwave is input from left side of the four-port PC cavity ((i) in Table. 2), the cavity becomes on-resonance state and the lightwaves can completely transmit to right side of the cavity without the reflection to left side. On the other hand, if an out-phase lightwave is input from left side of the cavity ((ii) in Table. 2), the resonant-mode is cancelled and the cavity becomes off-resonance state, which leads to the complete reflection to the left side without the transmission to right side. In this way, the four-port PC cavity can be operated as the linear logic gate.

3. Operation Principle and Numerical Results

3.1 Operation Principle

Before discussing the all-optical diode operation, we explain the linear characteristics of the all-optical diode. Let us first consider the backward propagation. Fig. 7(a) shows the illustration of the lightwave flow with the constellation diagram in the linear regime ($\gamma = 0$) when the lightwave is input from Port 4. The input lightwave splits into the upper and lower waveguides with the phase difference of $\pi/2$ in the 3-dB power divider, and then, the lower and upper waves have positive real

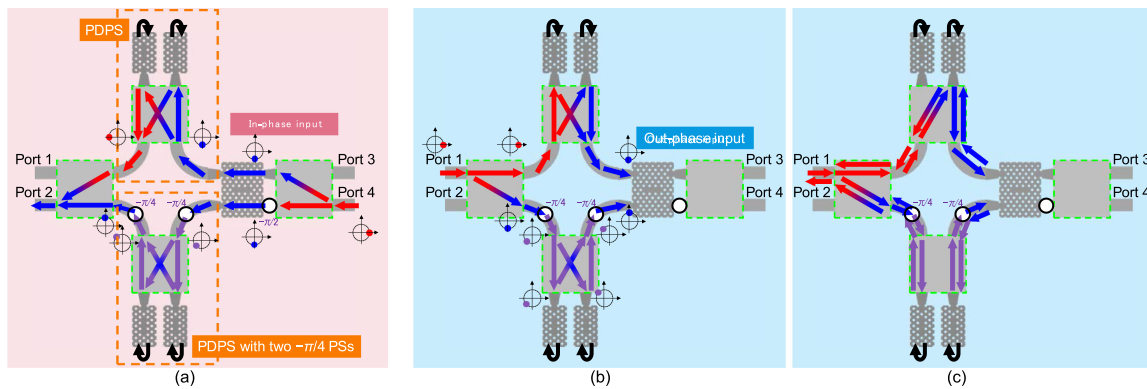


Fig. 7. Illustration of the lightwave flow with the constellation diagram in the linear regime ($\gamma = 0$) when the lightwave is input from (a) Port 4 (backward) and (b), (c) Port 1 (forward). In (b), the power flow until the lightwave input from Port 1 reaches the four-port PC cavity is shown, and in (c), the power flow until the reflected lightwave go back to Port 1 is shown.

($\theta = 0$) and negative imaginary ($\theta = -\pi/2$) amplitudes, respectively. Passing the $-\pi/2$ PS (delay line) in the lower waveguide, the in-phase wave reaches the four-port PC cavity, which can completely transmit to the left side of the four-port PC cavity. And then, the upper and lower waves pass through the PDPs. In the lower PDPs, two additional $-\pi/4$ PS are deployed. Therefore, before entering the left 3-dB power divider, the lower wave is $-\pi/2$ delayed than the upper wave, and hence, the entire power input from Port 4 escapes to Port 2. Whereas, in the case of the forward propagation, the device gives more complicated behavior. Noting that, in the linear regime, the lightwave input from Port 1 is completely reflected in the four-port PC cavity and go back to Port 1. As shown in Fig. 7(b), the power flow from Port 1 to the four-port PC cavity is similar to the case inputting from Port 4, however the out-phase wave reaches the four-port PC cavity, which leads to the complete reflection. Furthermore, the reflected upper and lower waves differently interfere with input waves in the upper and lower PDPs as shown in Fig. 7(c), and the entire power input from Port 1 eventually reflected to Port 1. According to the reciprocal theorem [24], we can find that the lightwave input from Port 2 should completely transmit to Port 4 and the lightwave input from Port 3 should completely reflect to Port 3, respectively.

From now on, we take the nonlinear effect into account. We should focus on the power flowing into two PDPs. Here we assume the input power is P . For the backward propagation, as shown in Fig. 7(a), each single-port PC cavities equally receive the power of $P/4$, which means that the even nonlinear phase shifts arise in four single-port PC cavities and do not affect the output power in the Port 2. Therefore, the phase difference of the lightwave entering the left 3-dB power divider keeps 90 degrees regardless of the amount of the nonlinear phase shift in each single-port PC cavity. Thus, the response in the backward transmission (from Port 4 to Port 1) is theoretically 0% even if the nonlinear effect is considered. On the other hand, for the forward propagation, the upper and lower PDPs have different behaviors in the nonlinear regime. As shown in Fig. 7(c), in the upper PDPs, the right single-port cavity only receive the power of P although the both cavity receive the power of $P/2$ equally in the lower PDPs. In addition, the total power entering single-port PC cavities is twice ($2P$) in the forward propagation rather than the backward propagation because the reflected wave as well as the input wave flows into PDPs. For example, we consider the case of the input power of $P = 0.72 \text{ W}/\mu\text{m}$. The upper-right single-port PC cavity receives the $0.32 \text{ W}/\mu\text{m}$, resulting in the reflection coefficient of $\exp(-2.0j)$ as can be seen in Fig. 4(b). Whereas, the lower two single-port PC cavities receives the $0.16 \text{ W}/\mu\text{m}$, resulting in the reflection coefficient of $\exp(+2.5j)$. As a result, the phase difference of about $\pi/2$ arises and the out-phase condition in the four-port PC cavity is obviously broken, which allows the forward transmission (from Port 1 to Port 4). Even if the reflection at the four-port PC cavity decreases up to 0% and the power flowing into the single-port PC cavities becomes $0.18 \text{ W}/\mu\text{m}$, the phase difference between upper and lower PDPs can be

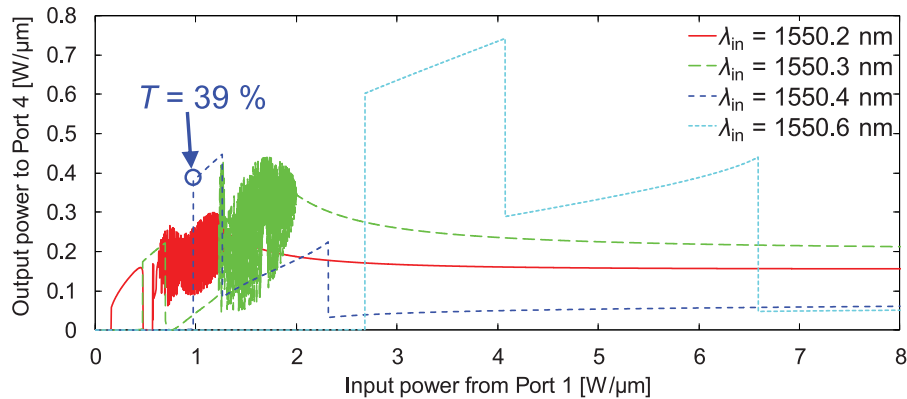


Fig. 8. Output power of port 4 as a function of the input power from port 1 in the proposed all-optical diode by calculating nonlinear CMT equations.

maintained due to the bistability. Although it is difficult to simply depict the nonlinear power flow for the forward propagation, it is sure that the forward transmission can be obtained in the nonlinear regime and the backward transmission is always 0% both in the linear and nonlinear regimes. This is the operation principle in our proposed all-optical diode.

One may think that the nonlinearity of the four-port PC cavity should be considered. In fact, the nonlinear phase shift is not negligible, however, especially in the backward propagation, it only affect the transmission from Port 4 to Port 2 and the reflection to Port 4, which prove that the backward transmission keeps 0%. We should also note that the “complete suppression of backward transmission” is genuine when Eqs. (5), (13) and (18) and three static PSs are precisely reproduced. For example, if the 3-dB divider or the static PSs does not precisely work, the backward transmission can arise. However, the wavelength dependences of these components are negligible compared to the PC cavities. According to Eqs. (13) and (18), there is no problem as long as the device is vertically symmetric except for the static PSs. The PS that is a delay line or a micro-heater has also trivial wavelength dependence compared to the other components. Therefore, we stated that our proposed device can block the backward transmission from Port 4 to Port 1 for any input wavelength and any input power.

3.2 Numerical Results

To investigate the nonlinear characteristics of the all-optical diode as shown in Fig. 1, we calculate Eqs. (7) and (15) for four single-port and one four-port PC cavities simultaneously and link the solutions with Eq. (5) for four 3-dB power dividers. Although we stated that the low Q -factor four-port PC cavity was available as a linear logic gate as shown in Table 2 when $\eta = -1$, the nonlinear characteristics of the four-port PC cavity is precisely analyzed in this section.

Fig. 8 shows the output power of port 4 as a function of the input power from port 1 in the proposed all-optical diode. The resonant characteristics of the four single-port PC cavities are the same as Fig. 4(b), and the resonant characteristics of four-port PC cavity is as follows: $\lambda_0 = 1550$ nm, $Q = 500$, $n_0 = 2.76$, and $\gamma = 10^{-4}$ $\mu\text{m}/\text{pJ}$. As seen in Fig. 8, the output power arises by increasing the input power. Although the unstable solution is obtained for the case of the small detuning condition ($\lambda_{\text{in}} < 1550.4$ nm), the stable output power of port 4 from port 1 can be obtained by setting sufficiently large detuning. If setting $\lambda_{\text{in}} = 1550.4$ nm and input power of 1.0 $\text{W}/\mu\text{m}$, we can obtain the maximum forward transmission of -4 dB (39%).

Figs. 9(a)–(f) show the transmission spectra of the proposed all-optical diode, where the input power is 0.02 , 0.1 , 1.0 , 1.5 , 3.0 , and 5.0 $\text{W}/\mu\text{m}$, respectively. The blue solid, red dotted, and green dotted lines denote Port 1 to Port 4, Port 1 to Port 2, and Port 4 to Port 2, respectively. As discussed in Subsection 3.1, the backward transmission (from port 4 to Port 1) is theoretically 0% ($-\infty$ dB)

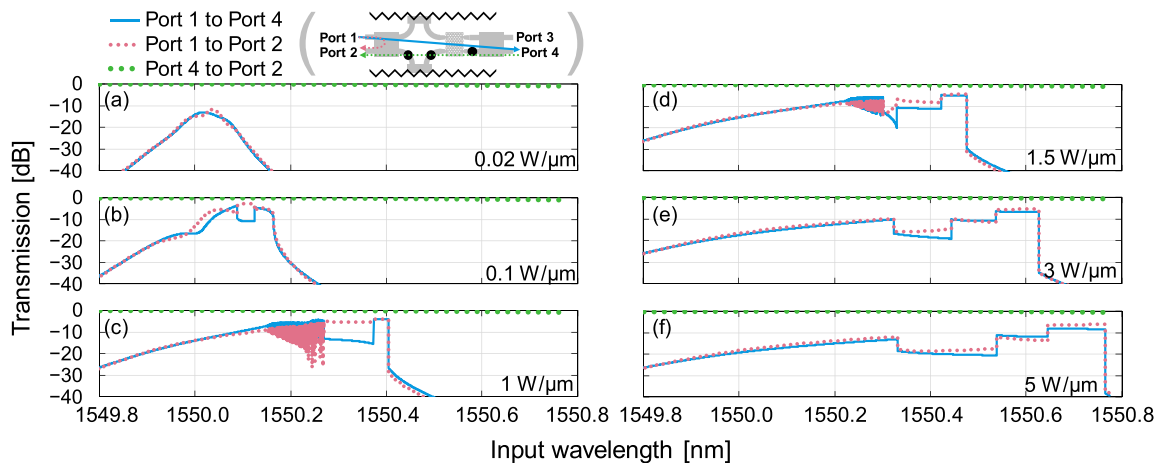


Fig. 9. Transmission spectra of the proposed all-optical diode for input power of (a) 0.02, (b) 0.1, (c) 1, (d) 1.5, (e) 3, and (f) 5 $W/\mu m$. The blue solid, red dotted, and green dotted lines denote Port 1 to Port 4, Port 1 to Port 2, and Port 4 to Port 2, respectively.

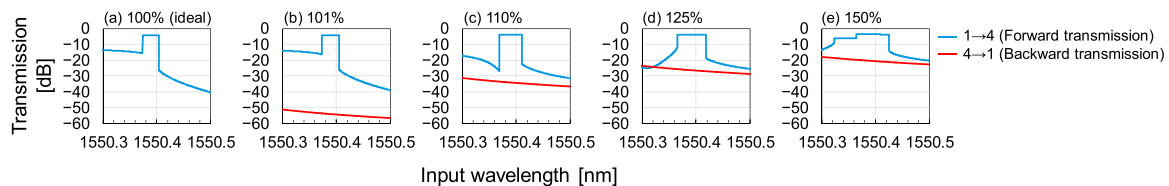


Fig. 10. Transmission spectra of the proposed all-optical diode for input power of 1 $W/\mu m$ when Q -factor of the upper-right single-port cavity is shifted to Q' , where $Q'/Q =$ (a) 1 (ideal), (b) 1.01, (c) 1.1, (d) 1.25, and (e) 1.5. The blue and red lines denote forward (Port 1 to Port 4) and backward (Port 4 to Port 1) transmission, respectively.

for any input condition and cannot be displayed in the graph. Instead, the lightwave input from Port 4 completely escapes to Port 2. For larger input power of 1.0 $W/\mu m$, we can see the flat forward transmission spectra that are formed by the mutual coupling between PC cavities. The unstable solutions disappear for larger input power of 3.0 $W/\mu m$. In addition, we can also see that the blue line and red line are with almost same transmission loss because the on-resonant condition in the four-port cavity, corresponding to in-phase input condition, gives transmission to Port 2 and Port 4 equally.

Fig. 10(a)–(e) show the transmission spectra of the proposed all-optical diode for input power of 1 $W/\mu m$ when the Q -factor of the upper-right single-port cavity is shifted to Q' , where $Q'/Q =$ 1 (ideal), 1.01, 1.1, 1.25, and 1.5. If set to $Q'/Q > 1$, the backward transmission arises due to breaking the condition as shown in Fig. 7(a). Nevertheless, as shown in Fig. 10(d), the flat spectrum of the -4 dB forward transmission and NTR of 20 dB can be obtained. Although the NTR becomes less than 20 dB for $Q'/Q = 1.5$, we can maintain the forward transmission of -4 dB. In addition, we change the Q -factors of two single-port cavities simultaneously. Fig. 11(a)–(c) show the transmission spectra of the proposed all-optical diode for input power of 1 $W/\mu m$ when the Q -factors of two single-port cavities is shifted to $Q' = 1.25Q$ where the changed cavities are the upper-right and upper-left cavities, upper-right and lower-right cavities, and upper-right and lower-left cavities, respectively. For the input wavelength of 1550.4 nm, the forward transmission of -4 dB and NTR of 20 dB can be obtained in each condition. It proves that the proposed device can tolerate the fabrication deviation to a certain degree. It also indicates the increase of Q -factor more than 50% gives too large backward transmission.

Finally, we perform the nonlinear analysis based on FDTD-BPM [25]. It can treat the rigorous electromagnetic field distribution in the whole system, in which the insertion loss between wire and

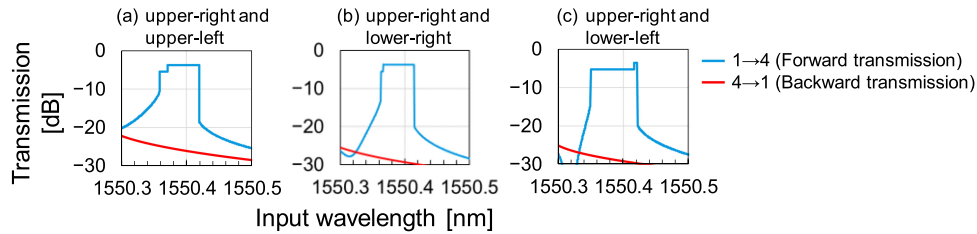


Fig. 11. Transmission spectra of the proposed all-optical diode for input power of $1 \text{ W}/\mu\text{m}$ when Q -factors of two single-port cavities is shifted to $Q' = 1.25Q$ where the changed cavities are (a) upper-right and upper-left cavities, (b) upper-right and lower-right cavities, and (c) upper-right and lower-left cavities, respectively.

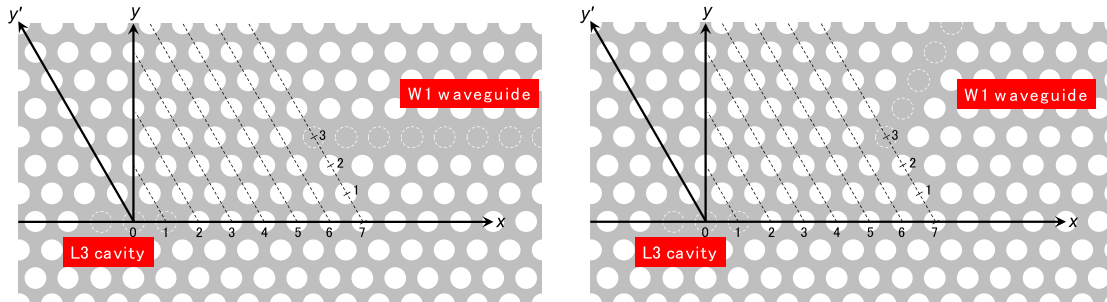


Fig. 12. Schematics of connection between L3 PC cavity and W1 PC waveguide with x - y' axis.

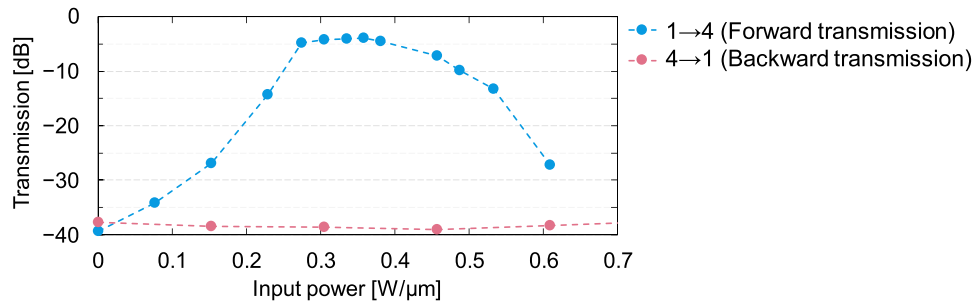


Fig. 13. Forward and backward transmission calculated by nonlinear FETD-BPM for $\lambda_{in} = 1560.56 \text{ nm}$.

PC waveguides, and the scattering loss in the PC cavities are taken into account. As the practical parameters, we choose the 400nm-width Si-wire waveguide and Si PC cavity with air cladding. The structural parameters of PC cavity are the same as Figs. 3(b) and (c). For adjusting the Q -factor of PC cavities, the distance between the PC cavity and the W1 waveguide is important. For the convenient expression, we use the x - y' axis as shown in Fig. 12(a), where y' -axis is 120-degree rotated x -axis and $(x, y') = (0, 0)$ is aligned to the center of the L3 PC cavity. In Fig. 12(a), the direction of line defect of L3 cavity is the same as W1 waveguide, whereas we can also deploy the W1 waveguide with 60-degree rotation as shown in Fig. 12(b). The edge of the line defect of W1 waveguide is positioned at $(x, y') = (7, 3)$ in both Figs. 12(a) and (b), and thus we call these PC cavities the $(7, 3, 0)$ and $(7, 3, 60)$ connection. For the single-port PC cavity, we choose PC cavity with $(7, 3, 0)$ connection, which has $Q_1 = 8200$ and $\omega_{in} = 2\pi c/1560.28 \text{ nm}$. Whereas, for the four-port PC cavity, we choose PC cavity with $(7, 3, 60)$ connection with vertical and horizontal mirror plane, which has $Q_4 = 670$ and $\omega_{in} = 2\pi c/1560.16 \text{ nm}$. For the effective connection, all W1 waveguides are connected to Si-wire waveguide with the four-period low-group-index W1 waveguide [26].

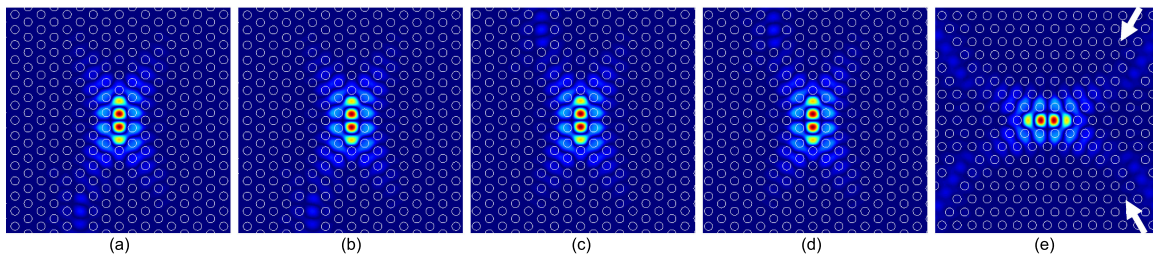


Fig. 14. Field distribution in the (a) upper left, (b) upper right, (c) lower left, (d) lower right single-port PC cavities and (e) four-port PC cavity for the backward propagation during the diode operation when the forward transmission is -4 dB.

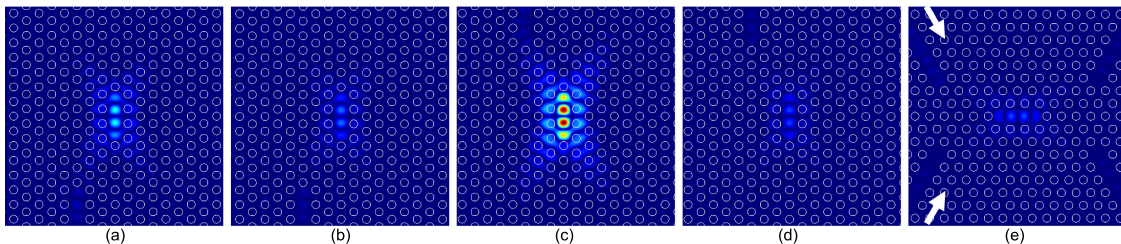


Fig. 15. Field distribution in the (a) upper left, (b) upper right, (c) lower left, (d) lower right single-port PC cavities and (e) four-port PC cavity for the forward propagation during the diode operation when the forward transmission is -4 dB.

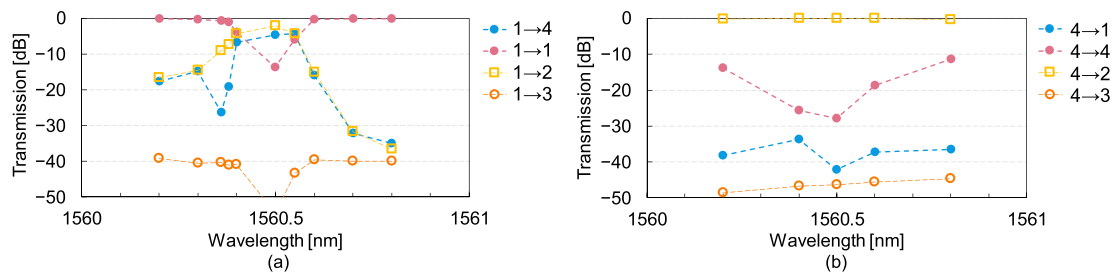


Fig. 16. Transmission spectra when the lightwave is input from (a) Port 1 and (b) Port 4.

Fig. 13 shows the forward and backward transmission calculated by nonlinear FDTD-BPM for $\lambda_{in} = 1560.56$ nm, where “ $n \rightarrow m$ ” in the legend denotes the transmission to the port m when the lightwave is input from Port n . We can see that the backward transmission becomes less than -35 dB for any input power, while the forward transmission of -4 dB is achievable when $\lambda_{in} = 1560.56$ nm and the input power is 0.3 W/ μm . The maximum transmission agrees with the numerical results by nonlinear CMT. The figure of merit of the all-optical diode, NTR, is about 35 dB. Figs. 14(a)–(e) show the field distribution in the PC cavities and for the backward propagation during the diode operation when the forward transmission is -4 dB. We can confirm that all single-port PC cavities are excited with almost the same amplitudes and the same nonlinear phase shift arises, which is proved that the backward transmission cannot be emerged. Figs. 15(a)–(e) show the field distribution for the forward propagation with the same condition as Fig 14(a)–(e). In contrast to the backward propagation, the power flowing into each cavity is different and it allows the power transmission to Port 4. Figs. 16(a) and (b) show the transmission spectra when the lightwave is input from Port 1 and 4, respectively. In the vicinity of 1560.5 nm, the high forward transmission ($1 \rightarrow 4$) is obtained. However, due to the complicated steady state, all of the forward input power does not reach Port 4 and the left power flows to Port 1 and 2. In particular, the transmission of $1 \rightarrow 1$ means the undesirable reflection. Although this reflection cannot be suppressed less than

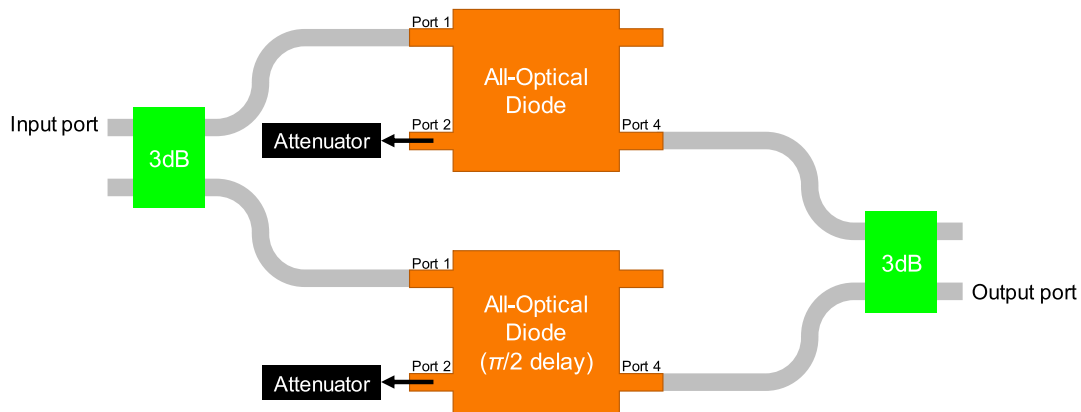


Fig. 17. Example of the device construction for input reflection suppression.

–15 dB as shown in Fig. 16(a), it can be suppressed by connecting two 3-dB power dividers and two all-optical diode as shown in Fig. 17. Let us emphasize that the backward transmission of $4 \rightarrow 1$ is suppressed less than –30 dB for any input wavelength even in the out of the resonant bandwidth. Such broadband characteristics of backward transmission in the nonlinear-resonator-based all-optical diode have not been reported excepted for our preliminary results [14]. As can be seen in Figs. 16(a) and (b), the bandwidth available for the diode-operation is about 0.2 nm due to the high Q -factor of four-port PC cavity ($\Delta\lambda = \lambda_0/Q = 0.19$). By choosing the lower Q -factor four-port PC cavity, the bandwidth becomes broader. For example, if we choose $Q_1 = 820$, the bandwidth becomes broad up to 2 nm.

4. Conclusion

In this paper, we present the all-optical diode suppressing broadband backward transmission using single- and four-port PC cavities. The key points in the proposed all-optical diode are exploiting the nonlinear phase shift from the PDPS and deploying the four-port PC cavity to generate the nonreciprocal characteristics. These device construction enables to eliminate the backward transmission in the nonlinear-resonator-based all-optical diode for any input power and any input wavelength. Furthermore, we demonstrate that the forward transmission of –4 dB and extremely large NTR can be achieved by rigorous nonlinear FETD-BPM analysis as well as nonlinear CMT.

References

- [1] K. Nozaki *et al.*, “Sub-femtojoule all-optical switching using a photonic-crystal nanocavity,” *Nature Photon.*, vol. 4, no. 7, pp. 477–483, Jul. 2010.
- [2] A. Martínez *et al.*, “Ultrafast all-optical switching in a silicon-nanocrystal-based silicon slot waveguide at telecom wavelengths,” *Nano Lett.*, vol. 10, no. 4, pp. 1506–1511, Apr. 2010.
- [3] M. F. Yanik, H. Altug, J. Vuckovic, and S. Fan, “Sub-micron all-optical memory and large scale integration in photonic crystals,” in *Proc. Conf. Lasers Electro Opt. Europe*, 2005, vol. 2739, no. 2003, p. 588.
- [4] E. Kuramochi *et al.*, “Large-scale integration of wavelength-addressable all-optical memories on a photonic crystal chip,” *Nature Photon.*, vol. 8, no. 6, pp. 474–481, May 2014.
- [5] Q. Xu and M. Lipson, “All-optical logic based on silicon micro-ring resonators,” *Opt. Exp.*, vol. 15, no. 3, pp. 924–929, Jan. 2007.
- [6] A. Fushimi and T. Tanabe, “All-optical logic gate operating with single wavelength,” *Opt. Exp.*, vol. 22, no. 4, pp. 4466–4479, Feb. 2014.
- [7] M. Xu, J. Wu, T. Wang, X. Hu, X. Jiang, and Y. Su, “Push-pull optical nonreciprocal transmission in cascaded silicon microring resonators,” *IEEE Photon. J.*, vol. 5, no. 1, Feb. 2013, Art. no. 2200307.
- [8] Y. Zhang *et al.*, “Silicon optical diode based on cascaded photonic crystal cavities,” *Opt. Lett.*, vol. 39, no. 6, pp. 1370–1373, Mar. 2014.
- [9] Y. Yu, Y. Chen, H. Hu, W. Xue, K. Yvind, and J. Mork, “Nonreciprocal transmission in a nonlinear photonic-crystal Fano structure with broken symmetry,” *Laser Photon. Rev.*, vol. 9, no. 2, pp. 241–247, Mar. 2015.

- [10] L. Fan, L. T. Varghese, J. Wang, Y. Xuan, A. M. Weiner, and M. Qi, "Silicon optical diode with 40 dB nonreciprocal transmission," *Opt. Lett.*, vol. 38, no. 8, pp. 1259–1261, Apr. 2013.
- [11] Y. Shi, Z. Yu, and S. Fan, "Limitations of nonlinear optical isolators due to dynamic reciprocity," *Nature Photon.*, vol. 9, no. 6, pp. 388–392, Jun. 2015.
- [12] T. Sato, T. Fujisawa, and K. Saitoh, "Design of a high-forward-transmission all-optical diode based on cascaded side-coupled photonic crystal cavities," *J. Opt. Soc. Amer. B*, vol. 34, no. 12, pp. 2493–2500, Dec. 2017.
- [13] C. Li, M. Wang, and J.-F. Wu, "Broad-bandwidth, reversible, and high-contrast-ratio optical diode," *Opt. Lett.*, vol. 42, no. 2, pp. 334–337, Jan. 2017.
- [14] T. Sato, T. Fujisawa, and K. Saitoh, "Novel all-optical diode based on single-port and four-port photonic crystal cavities," in *Proc. 23rd Opto Electron. Commun. Conf.*, 2018, p. 4D2–2.
- [15] P. A. Besse, M. Bachmann, H. Melchior, L. B. Soldano, and M. K. Smit, "Optical bandwidth and fabrication tolerances of multimode interference couplers," *J. Lightw. Technol.*, vol. 12, no. 6, pp. 1004–1009, Jun. 1994.
- [16] L. B. Soldano and E. C. M. Pennings, "Optical multi-mode interference devices based on self-imaging: Principles and applications," *J. Lightw. Technol.*, vol. 13, no. 4, pp. 615–627, Apr. 1995.
- [17] P. E. Morrissey, H. Yang, R. N. Sheehan, B. Corbett, and F. H. Peters, "Design and fabrication tolerance analysis of multimode interference couplers," *Opt. Commun.*, vol. 340, pp. 26–32, Nov. 2015.
- [18] H. Guan *et al.*, "Compact and low loss 90° optical hybrid on a silicon-on-insulator platform," *Opt. Exp.*, vol. 25, no. 23, pp. 28957–28968, Nov. 2017.
- [19] H. A. Haus, *Waves and Fields in Optoelectronics*. Englewood Cliffs, NJ, USA: Prentice-Hall, 1984.
- [20] C. R. Doerr *et al.*, "Bending of a planar lightwave circuit 2 × 2 coupler to desensitize it to wavelength, polarization, and fabrication changes," *IEEE Photon. Technol. Lett.*, vol. 17, no. 6, pp. 1211–1213, Jun. 2005.
- [21] G. F. R. Chen, J. R. Ong, T. Y. L. Ang, S. T. Lim, C. E. Png, and D. T. H. Tan, "Broadband silicon-on-insulator directional couplers using a combination of straight and curved waveguide sections," *Sci. Rep.*, vol. 7, no. 7246, pp. 1–8, Aug. 2017.
- [22] A. Chutinan and S. Noda, "Waveguides and waveguide bends in two-dimensional photonic crystal slabs," *Phys. Rev. B*, vol. 62, no. 7, pp. 4488–4492, Aug. 2000.
- [23] T. Uesugi, B.-S. Song, T. Asano, and S. Noda, "Investigation of optical nonlinearities in an ultra-high-Q Si nanocavity in a two-dimensional photonic crystal slab," *Opt. Exp.*, vol. 14, no. 1, pp. 377–386, Jan. 2006.
- [24] D. Jalas *et al.*, "What is — and what is not — an optical isolator," *Nature Photon.*, vol. 7, no. 8, pp. 579–582, Jul. 2013.
- [25] T. Fujisawa and M. Koshiba, "Time-domain beam propagation method for nonlinear optical propagation analysis and its application to photonic crystal circuits," *J. Lightw. Technol.*, vol. 22, no. 2, pp. 684–691, Feb. 2004.
- [26] J. P. Hugonin, P. Lalanne, T. P. White, and T. F. Krauss, "Coupling into slow-mode photonic crystal waveguides," *Opt. Lett.*, vol. 32, no. 18, pp. 2638–2640, Sep. 2007.